Thermochronology of upper crustal rocks in the Wood Hills, Nevada: Documenting exhumation in the U.S. Cordillera

Nicole Gonzalez
Department of Geological Sciences
University of Colorado Boulder

November 6, 2019

Thesis Advisor:
Dr. James Metcalf, Research Associate, Department of Geological Sciences

Defense Committee:
Professor Rebecca Flowers, Department of Geological Sciences
Professor Brian Hynek, Department of Geological Sciences
Instructor Sarah Kelly, Department of Geography

ABSTRACT

The metamorphic core complexes of the Basin and Range Province record a long and complex geologic history that includes contraction and crustal shortening followed by extensional deformation and thinning. Many studies using a wide range of methods have attempted to uncover how regional extensional collapse of the crust initiated. Previous work on high temperature processes has documented older, Cretaceous to Eocene (~70 – 34 Ma) deformation, whereas studies of shallower crust (using low temperature thermochronology and basin analysis) highlight more recent, Miocene (~15 Ma) processes. In order to address a gap in the thermochronologic record across the Ruby Mountains – East Humboldt Range – Wood Hills metamorphic core complex in northeastern Nevada, we use zircon and apatite (U-Th)/He thermochronology within a well-understood structural framework from samples in the Wood Hills to document the cooling and exhumational history of the shallower parts of the core complex.

New zircon and apatite (U-Th)/He dates from the Wood Hills record late Eocene to late Miocene cooling through a zircon He closure temperature of ~150 - 180 °C and an apatite He closure temperature of ~60 - 70 °C. These results are consistent with previous studies using 40Ar/39Ar and (U-Th)/He thermochronology that suggest that cooling related to extensional exhumation in the Wood Hills occurred during at least two cooling events: one at ~40 Ma and another beginning at ~20 Ma. Furthermore, apatite dates obtained from the northern Wood Hills suggest an exhumational cooling event continued until ~10 Ma, similar to apatite (U-Th)/He dates from throughout the complex. Date-eU correlations coupled with thermal modeling aids to support a multi-step exhumation path in the Wood Hills that has also been largely documented in other parts of the metamorphic core complex.

INTRODUCTION

The Basin and Range Province is defined by alternating approximately north-south trending valleys and ranges formed as a result of extensional deformation and thinning preceded by contraction and crustal shortening. While plenty of studies have attempted to uncover how regional extensional collapse of the crust initiated through a wide range of methods, debate regarding timing and rate of deformation still exists. Fundamentally, evidence from different depths of the crust have yielded differing interpretations, with evidence from the deeper earth documenting older, Cretaceous to early Paleogene (~70 Ma) deformation, whereas studies of the shallower crust highlight more recent, Miocene (~15 Ma) processes. Since the metamorphic core complexes of the U.S. Cordillera expose large and relatively continuous sections of the crust, these updomed structures are essential for understanding the tectonic mechanisms that drive the transition from widespread crustal shortening to regional crustal thinning.

In this study, we attempt to fill a gap in the thermochronometric record across the Wood Hills, Nevada. In addition, we focus on better understanding the exhumation path of this complex following peak metamorphism by creating thermal models using HeFTy to test thermal history hypotheses. Structural and metamorphic relationships highlighted in the Wood Hills coupled with our thermochronologic data serve to construct a more complete age pattern in the Wood Hills. Our data will be integrated with complementary and parallel studies in the Ruby Mountains and East Humboldt Range metamorphic core complexes at both the University of Colorado- Boulder and the University of Dayton in an effort to determine when and how quickly the region shifted from contraction to extension.

BACKGROUND

Geologic History of the Ruby Mountains - East Humboldt Range - Wood Hills metamorphic core complex (REHW):

The REHW consists of rock units that are Neoarchean to Holocene in age. The Ruby Mountains- East Humboldt Range (RM-EHR) located on the western portion of the region are dominated by high-grade metamorphic and associated igneous rocks (Figure 1; McGrew and Snoke, 2015), while the Wood Hills and Pequop Mountains located on the eastern side are of lower metamorphic grades and record Mesozoic metamorphism and deformation (Thorman, 1970; Camilleri, 1994).

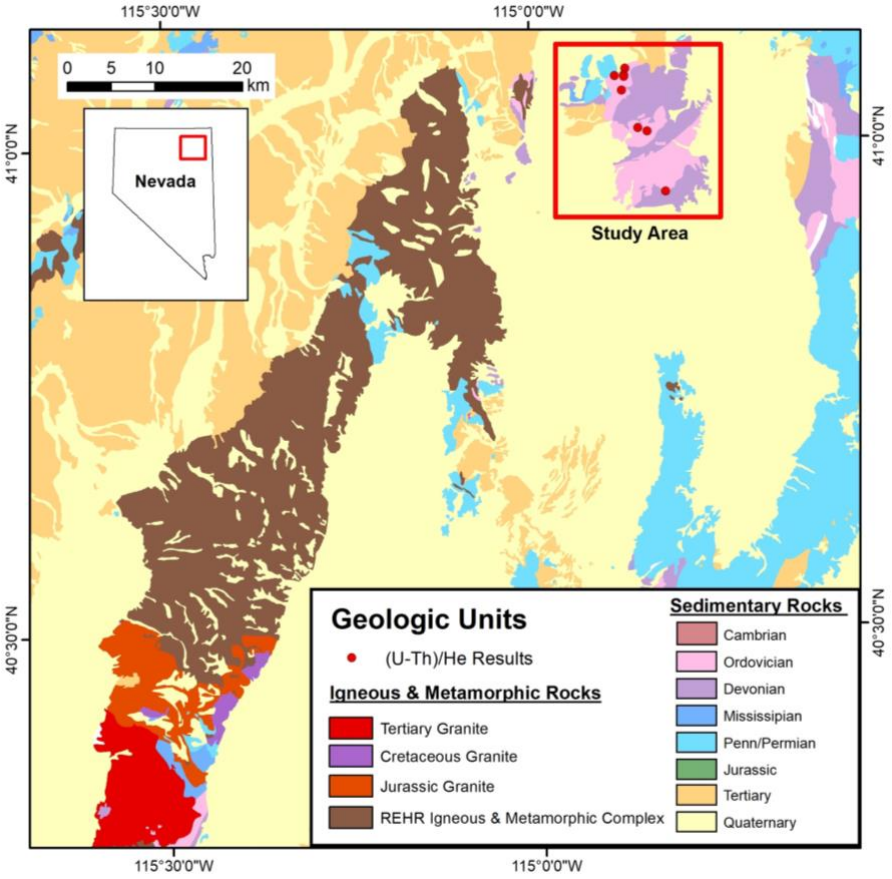

Figure 1. *A simplified geologic map of the Ruby Mountains – East Humboldt Range – Wood Hills metamorphic core complex (REHW). The box highlights my study area, the Wood Hills. For a simplified geologic map of the Wood Hills, see Figure 2.*

The rocks within the REHW consist of Neoarchean to early Paleoproterozoic basement, Neoproterozoic to Paleozoic metamorphosed shelf margin sediments (Snee et al., 2016) and Tertiary volcanic and clastic rocks (Camilleri and Chamberlain, 1997). Pre-Cenozoic rocks comprised of ocean basin and continental slope sedimentary rocks were emplaced over shelfal rocks deposited during the Mississippian Antler orogeny (Lund Snee et al., 2016). The earliest phase of extension was accompanied by voluminous ignimbrite deposits and exhumation of metamorphic core complexes (Satarugsa and Johnson, 2000). In the northern Ruby Mountains, Paleozoic sediments were buried, equivalent to ~9 kb, and metamorphosed during Mesozoic crustal shortening; however, those same rocks in the southern Ruby Mountains were never buried below stratigraphic depths prior to exhumation (Colgan et al., 2010). Exhumation of these rocks in the southern Ruby Mountains was caused largely by Cenozoic normal slip on a now shallowly west-dipping (~20°) brittle fault system that overprints a mylonitic shear zone (Colgan et al., 2010). These rocks are presumed to be exhumed as early as the Eocene with the fastest and most significant exhumation having occurred in the Oligocene and early Miocene (Colgan et al., 2010).

The Humboldt Formation of Miocene age can be subdivided into two units separated by the middle Miocene Willow Creek rhyolite suite (McGrew and Snoke, 2015). The lower unit distinguished by pale-green to pale-yellow slopes above tuffaceous siltstone, siliceous siltstone, and very fine sandstone yield a $^{40}Ar/^{39}Ar$ age of 15.52 ± 0.12 Ma (McGrew and Snoke, 2015). The upper unit (stratigraphically above the Willow Creek suite) consists of tuffaceous sandstone and siltstone, conglomerate, limestone, tuff, and vitric ash (McGrew and Snoke, 2015). In the conglomeritic rocks, Eureka Quartzite and calcite marble clasts are presumed to be from a source of unroofing of a metamorphic terrain like the Wood Hills (Thorman 1970; Camilleri, 2010).

Since these clasts are not mylonitic, it is assumed that the early Oligocene mylonitic shear zone was not exposed at the time of the Humboldt Formation upper unit's deposition. The modern faults bounding the East Humboldt Range are the youngest segments of the Mary's River fault system, which largely accomplished the exhumation of the metamorphic terrain of the East Humboldt Range and Wood Hills (Camilleri and Chamberlain, 1997). The Humboldt Formation represents part of the synextensional basement that formed along the Mary's River fault system (Camilleri and Chamberlain, 1997).

The Wood Hills expose the intermediate grade, mid to upper crustal parts of the metamorphic core complex. They are composed of metamorphosed and unmetamorphosed Paleozoic packages and Cenozoic volcanic strata that are structurally divided by a low angle normal fault known as the Wood Hills fault (Camilleri, 2010). Repetition of layers across low angle faults in the Wood Hills and Pequops suggests that duplication of strata by thrust faulting occurred prior to extension (Camilleri and Chamberlain, 1997). At least two episodes of thrusting are inferred: the first resulted in widespread late Cretaceous (~154 – 84 Ma) tectonic burial of the middle crust and duplicated the miogeocline and the second created the Cretaceous age (~84 – 75 Ma) Independence thrust fault in the Pequop Mountains (Camilleri and Chamberlain, 1997). Based on U-Pb data published by Camilleri and Chamberlain (1997), metamorphism in northeastern Nevada began sometime after 154 ± 5 Ma and continued until the last pulse of crustal shortening by the Independence thrust between 84 and 75 Ma. The Pequop fault initialized extension in the region prior to 75 Ma and the Mary's River fault system drove the final exhumation of the Mesozoic crust sometime between 41 Ma to recent time (Camilleri and Chamberlain, 1997).

SAMPLES

My interest area spans a northwest to southeast trending transect of the Wood Hills (Figure 2). In 2018, I collected and separated two samples from the field: RGDJ18-11 and RGDJ18-12. RGDJ18-11 yielded no apatite and the zircons were in poor condition and produced unreliable results, therefore that sample was not used in this analysis. RGDJ18-12 yielded no apatite or zircon and was also excluded from this study. Unfortunately, more sampling was not possible due to property ownership and access issues. Instead, I analyzed and/or separated samples collected by other colleagues in previous years, three of which were collected in 2017: RGD17-31, RGD17-32, RGD17-35. Samples JR_D, JR_J, JR_K, JR_O, and JR_S were originally collected and analyzed by Franklin D. Wolfe, an undergraduate student at Washington and Lee University; however, I have acquired new zircon data for JR_J, JR_O, JR_S that strengthen my interpretations and allow for more complete thermal modeling. Finally, sample 10C was obtained and separated by Dr. Phyllis A. Camilleri and handpicked by me to obtain zircon and apatite data.

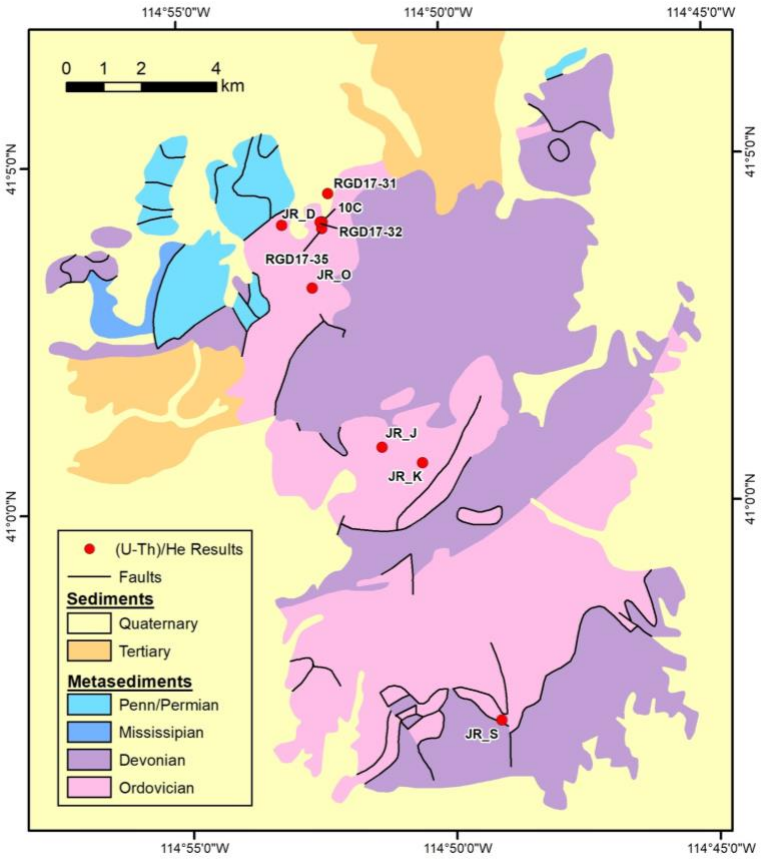

Figure 2. *A simplified geologic map of the Wood Hills, Nevada with each sample labeled.*

Most of the samples were taken from the Eureka Quartzite, an Ordovician age white quartzite with sparse gray streaks (Figure 3; Camilleri, 2010). RGD17-31 was collected from

brecciated Eureka Quartzite that was not mylonitized. RGD17-32 was acquired from mylonitized Eureka Quartzite and RGD17-35 was collected from a granite pod that contained large phenocrysts and mafic minerals. 10C was sampled from a granite exposure very close to RGD17-32.

Figure 3. *Eureka Quartzite*

METHODS

Mineral Separation Methods

Zircon and apatite separates were obtained using standard mineral separation procedures. For each sample collected in the field, about 4 kg of rock was crushed and ground down in a jaw crusher and Bico Rock Pulverizer. After pulverization, samples were separated using a 500-micron sieve. The <500-micron separate was then passed through a Wilfley Table where grains were separated based on density. The heavy separates were dried in an oven and then a hand magnet was used to remove highly magnetic material. After, the samples were passed through a Frantz Magnetic Separator at two magnetic amperage intensities (0.35, 0.6). Finally, non-magnetic separates were further divided using Lithium Metatungstate which has a density of 2.9 g/cc and can float off quartz and feldspar.

Mineral grains were handpicked at a Leica M165 binocular microscope and assessed for

quality. For apatite, quality is assessed on how large the crystal is, its euhedral shape, minimal abrasions on the surface of the crystal, and most importantly an absence of mineralized cracks or mineral inclusions. The minimum diameter for an apatite that can be accurately dated is about ~60 μm. For zircon, quality is assessed based on a euhedral shape and a minimum diameter of ~50 μm. Once desired grains were selected, each grain was individually packed in a niobium tube and each packet was loaded into an ASI Alphachron He extraction and measurement line. The packet was placed in the UHV extraction line (~3 X 10^{-8} torr) and heated with a 25W diode laser to ~800-1100°C for 5 to 10 minutes to extract the radiogenic ^{4}He. The degassed ^{4}He was then spiked with approximately 13 ncc of pure ^{3}He, cleaned via interaction with two SAES getters, and analyzed on a Balzers PrismaPlus QME 220 quadrupole mass spectrometer. This procedure was repeated at least once to ensure complete mineral degassing. Degassed grains were then removed from the line, and taken to a Class 10 clean lab for dissolution. Apatite grains, still enclosed in the Nb tubes, were placed in 1.5 mL Cetac vials, spiked with a ^{235}U - ^{230}Th – ^{145}Nd tracer in HNO_3, capped, and baked in a lab oven at 80°C for 2 hours.

Zircons were dissolved using Parr large-capacity dissolution vessels in a multi-step acid-vapor dissolution process. Grains were spiked with a ^{235}U - ^{230}Th - ^{145}Nd tracer, mixed with Optima grade HF, stacked in a 125 mL Teflon liner, placed in a Parr dissolution vessel, and baked at 220°C for 72 hours. The vials were dried down on a 90°C hot plate and underwent a second round of acid-vapor dissolution, this time with 6N Optima grade HCl in each vial and the grains were baked at 200°C for 24 hours. Vials were dried a second time on a hot plate and a 7:1 HNO_3:HF mixture was added to each vial. The vial was capped and cooked at 90°C for 4 hours. Once minerals were dissolved, they were diluted with 1 to 3 mL of doubly-deionized water, and taken to the ICP-MS lab for analysis. Sample solutions, along with normal solutions and blanks,

were analyzed for U, Th, and Sm content using an Agilent 7900 quadrupole ICP-MS. After the U, Th, and Sm contents were measured, He dates and all associated data was calculated on a custom spreadsheet using the methods described in Ketcham et al., (2011). The natural occurring 238U/235U ratio used in data reduction is 137.818 per Hiess et al. (2012). Long term averages of Fish Canyon Tuff zircons and Durango fluorapatites run in the CU TRaIL are 28.7 ± 1.8 Ma (n=150) and 31.1 ± 2.1 (n=85), respectively.

(U-Th)/He Thermochronology

Thermochronology is an isotopic dating methods that calculates dates by using the ratio between radioactive parent and stable daughter isotopes. Radioactive decay occurs when unstable radioactive parent isotopes (^{238}U, ^{235}U, ^{232}Th, ^{147}Sm) decay into stable daughter isotopes, which can either accumulate over time or be lost due to diffusion (Metcalf and Flowers, 2019, in press). ^{4}He is produced during the alpha decay of these parent isotopes and accumulates in a crystal over geologic time. When ^{4}He is retained in the crystal lattice at relatively low temperatures, it is referred to as "closed system" behavior (Metcalf and Flowers, 2019, in press). At higher temperatures, ^{4}He can diffuse instantaneously out of the crystal lattice and is then considered an "open system" (Metcalf and Flowers, 2019, in press). The transition from open to closed behavior is thermally controlled and ideally related to cooling through a narrow temperature window known as the closure temperature (T_c). In most geologic systems, the transition from open to closed behavior is not instantaneous, but rather occurs over a temperature range in which ^{4}He is partially retained (Wolf et al., 1998). It is important to note that a mineral may transition from open to closed behavior, and vice versa, multiple times throughout its life; therefore, the calculated date records the integrated thermal history of the sample. In order to

obtain information on a sample's thermal history, we performed (U-Th)/He dating of apatite and zircon. Apatite and zircon are ideal thermochronometers because they have an abundance of parent atoms and their diffusion kinetics are well understood.

As a result of the high kinetic energy with which α-particles are emitted from their parent nuclides, they may be lost from grains as a result of α-ejection (Farley et al., 1996). Unlike ^{4}He lost due to diffusion, these ejected atoms do not provide information on a sample's thermal history and thus a correction must be made to account for this effect (Metcalf and Flowers, 2019, in press). The "raw" date is calculated using the age equation, and the "corrected" date is determined by estimating and accounting for the amount of ^{4}He lost due to α-ejection.

The zircon system behaves similarly to that of apatite. The closure temperature of zircon without significant radiation damage is ~150 - 180°C (Reiners and Farley, 1999). Realistic and accurate interpretations using zircon as a thermochronometer involves understanding how He diffusivity is affected by temperature, crystallographic orientation, and radiation damage (Guenthner et al., 2013). Radiation damage is caused by self-irradiation and can be annealed at high temperatures. To roughly predict the extent of radiation damage in a grain, we calculate time-integrated self-irradiation doses, known as alpha doses (Guenthner et al., 2013). The alpha doses calculated from He ages reflect the total accumulation of alpha decay events since damage was last annealed (Guenthner et al., 2013). Like apatite, increasing radiation damage leads to the disruption of diffusion "fast-paths", which makes a He atom's path more tortuous thereby causing a decrease in the effective diffusivity of a grain (Flowers et al., 2009; Guenthner et al., 2013). Unlike apatite, when zircons accumulate very high levels of radiation damage, diffusivity dramatically increases, lowering the mineral's closure temperature.

HeFTy Thermal Modeling Methods

HeFTy is a windows-based computer modeling program developed by Dr. Richard Ketcham that models and helps users interpret thermochronologic data. Thermochronologic dates do not typically represent the date at which a mineral crystallized, but rather document the entire thermal history of that mineral since the accumulation of radiation damage and retention of helium. Since there are an enormous number of thermal histories that can satisfy a thermochronometric date, HeFTy provides a way to address geologic constraints within our data and explore a range of interpretations that satisfy those constraints. The program can produce both forward and inverse models. The forward model calculates a date based on a particular time-temperature path. The inverse model produces a collection of time-temperature paths within a set of prescribed geologic constrains that reasonably explain a date. In this study, we used inverse modeling to better understand the exhumational path of the metamorphic core complex in the Wood Hills based on the dates obtained from my zircon and apatite separates.

I modeled RGD17-31, 10C, and JR_J using the same methodology. Each sample included two ZHe age inputs determined by averaging similar results: one with high eU (1000 > ppm) values and the other with low eU (< 1000 ppm) values making sure that grains in both groups were in the same radius size range. Grains with an abnormal radius size outside the spread of data were not included in the averages. The average values for radius, uranium, thorium, samarium, raw date, and corrected date were calculated for both helium models and those averages were input into HeFTy. For zircon, the Guenthner (2013) diffusion model was selected. For the average raw date, a geologically reasonable uncertainty of 10% was used. Each model attempted 10,000 different time-temperature paths and only those that are consistent with the measured data are displayed.

Based on $^{40}Ar/^{39}Ar$ data from biotite and muscovite in metapelite, the model (Figure 14, 15) was constrained to cool through ~300° ± 20 C between 56 and 47 Ma (Thorman and Snee, 1988). My second constraint initialized the model between 85 and 80 Ma at ~340° C since timing of peak metamorphism in the Wood Hills is inferred at 84 Ma according to U-Pb sphene dates published by Camilleri and Chamberlain, 1997. The near surface constraint is based on the East Humboldt formation data that suggests most of the complex was cooling through ~20°C and exposed at the surface by ~17 Ma (Colgan et al., 2010).

RESULTS

Fifty ZHe dates (Table 1) from nine samples display large spreads in eU (U + 0.235 X Th, a proxy for radiation damage; Flowers et al., 2009) and variable patterns in date-eU space. The ZHe dates range from 18 to 44 Ma and eU spans from 47 ppm to concentrations as high as 35133 ppm. ZHe ages tend to young to the northwest of the Wood Hills, roughly parallel to the transport direction of the complex, and are summarized accordingly. The farthest south sample, JR_S (Figure 4A, 4B), has seven zircons that show a flat date-eU correlation across a 47 to 396 eU range with a mean date of 39.0 ± 1.8 Ma. JR_K (Figure 5A,5B) was sampled in the middle of the range and shows a weak negative date-eU correlation with eU concentrations below 250 ppm that yield a mean date of 34.3 ± 1.6 Ma. JR_J (Figure 6A, 6B), collected northwest of JR_K, displays a negative eU-date correlation across a 79 to 718 eU range and yields dates that span from 22 to 44 Ma. JR_O (Figure 7A, 7B) shows no date-eU correlation across a limited eU range of 107 to 221 ppm and has dates that span from 23 to 30 Ma. One solitary zircon has an eU concentration of 670 ppm, but yields a date within the age range of the rest of the sample.

The following five samples were collected within close proximity of one another in the northwestern portion of the range, but show varying date-eU patterns. RGD17-31 (Figure 8A, 8B), the northernmost sample, shows a flat date-eU correlation despite the large eU range from 65 to 1750 ppm. RGD17-35 (Figure 9A, 9B) displays a negative date-eU correlation with the exception of RGD17-35_z04. RGD17-35 has the greatest eU range from 6489 to 35133 Ma and yields dates that span from 21 to 42 Ma. RGD17-32 (Figure 10A, 10B) lies very close to the aforementioned sample, but only has three zircons that have dates ranging from 19 to 28 Ma. 10C was likely sampled from the same granite as RGD17-32 and shows both a positive and negative date-eU correlation. 10C (Figure 11A, 11B) has a high eU range from 5069 to 13850 ppm and yields dates that span from 24 to 43 Ma. Finally, JR_D (Figure 13A, 13B) has two zircons with low eU that yield a ~42 Ma date and one solitary grain with an eU concentration of 471 ppm that has a 22.9 ± 0.34 Ma date.

Four AHe dates (Table 2) from sample 10C (Figure 12A, 12B) show a negative date-eU correlation with an eU range of 33 to 472 ppm and yield dates that span from 7 to 13 Ma.

Date-eU and Date-rs Plots

Figure 4A

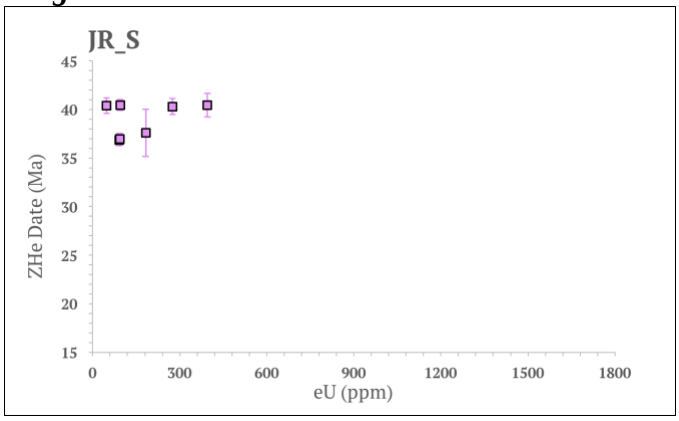

Figure 4B

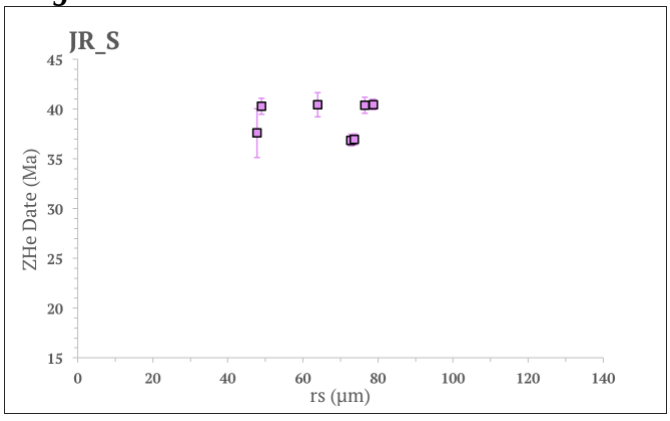

Figure 5A

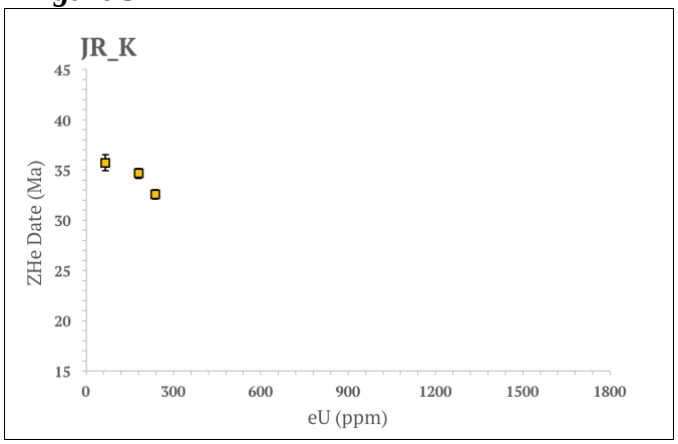

Figure 5B

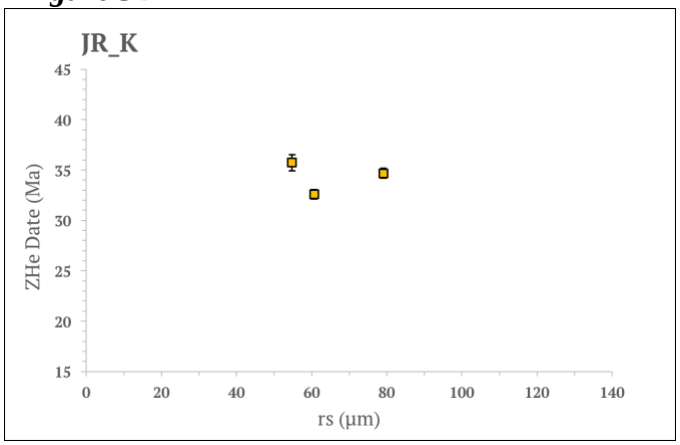

Figure 6A

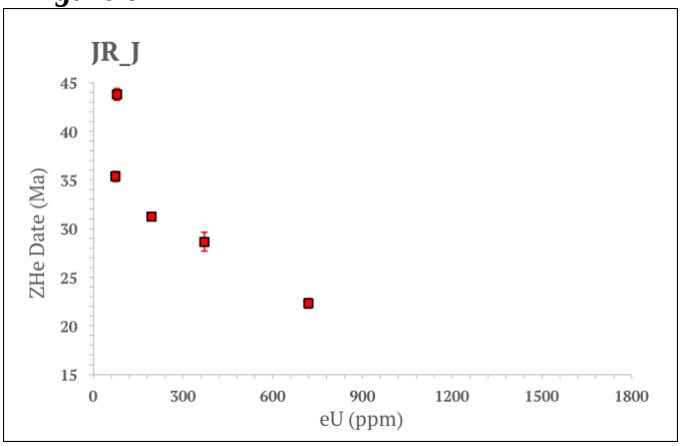

Figure 6B

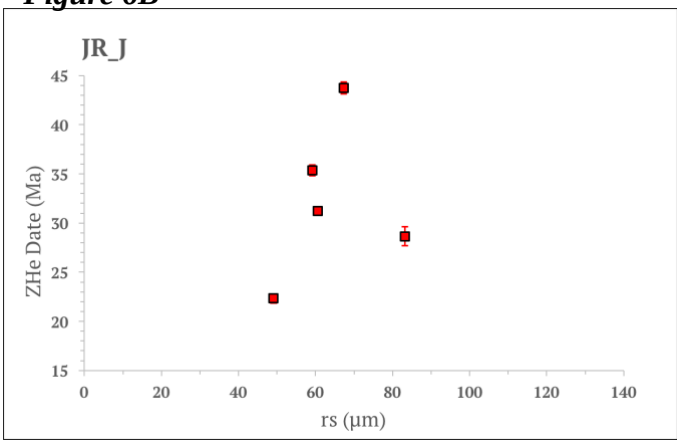

Figure 7A

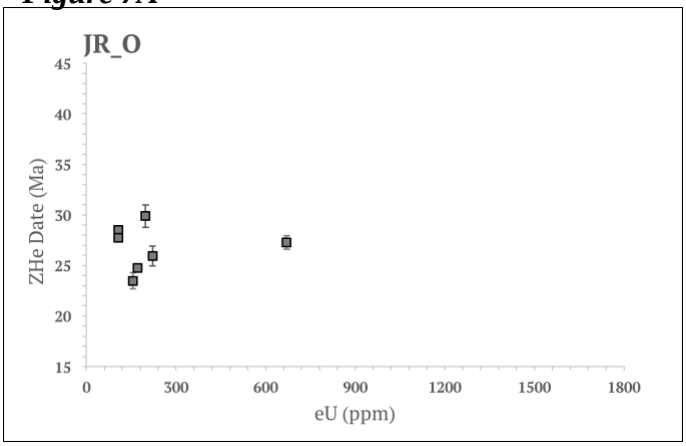

Figure 7B

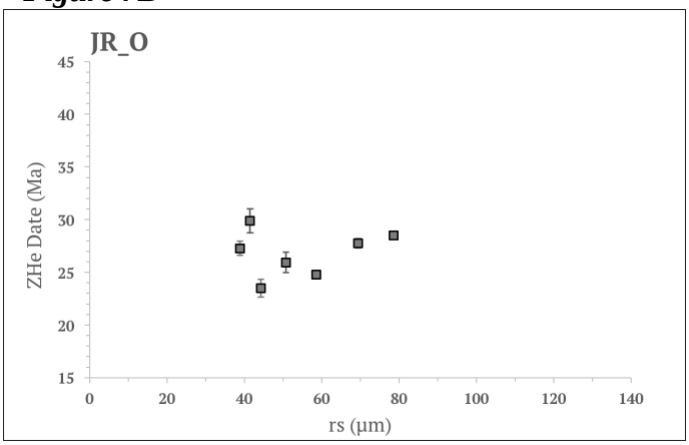

Figure 8A

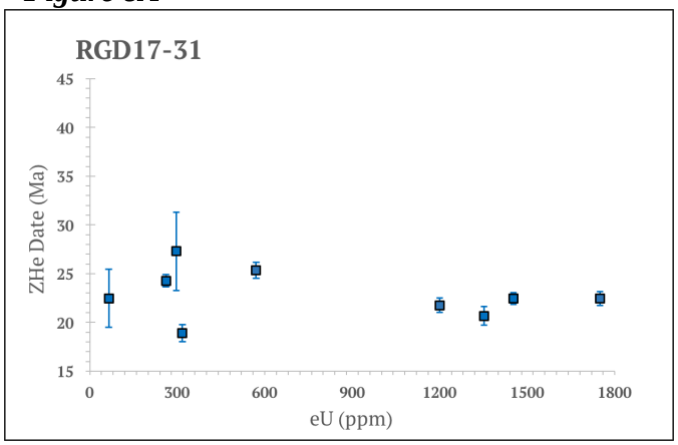

Figure 8B

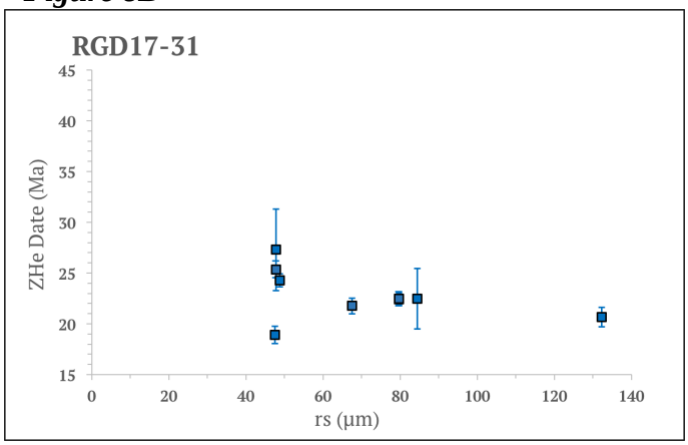

Figure 9A

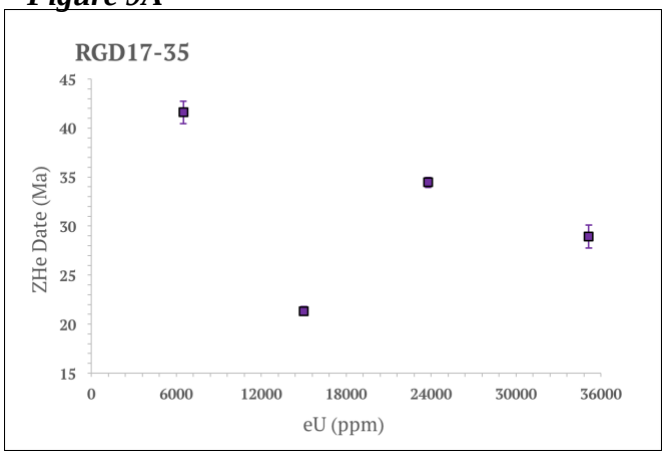

Figure 9B

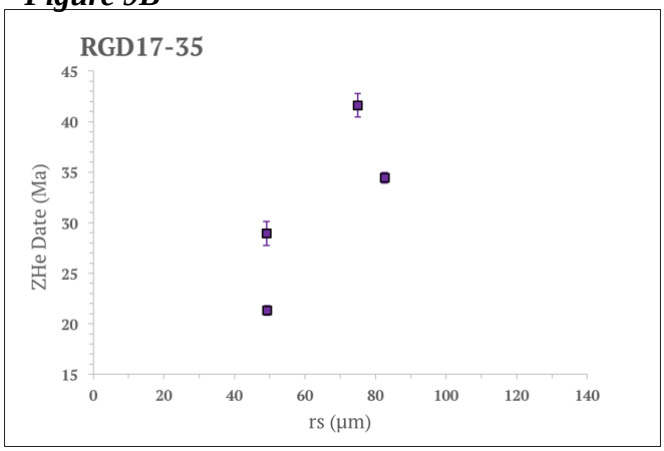

Figure 10A

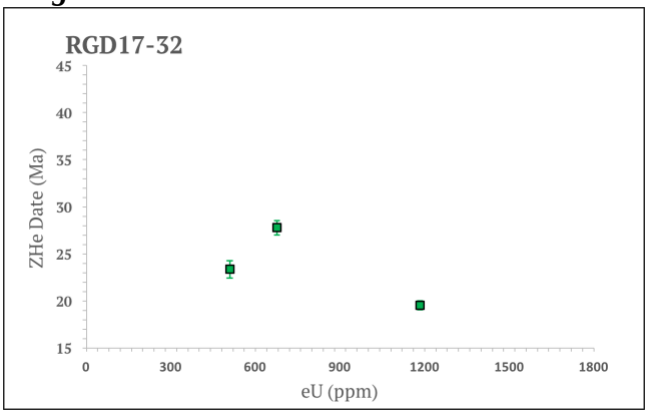

Figure 10B

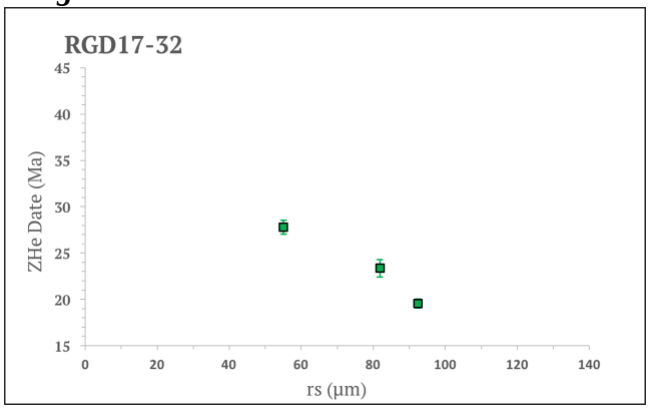

Figure 11A- Zircon

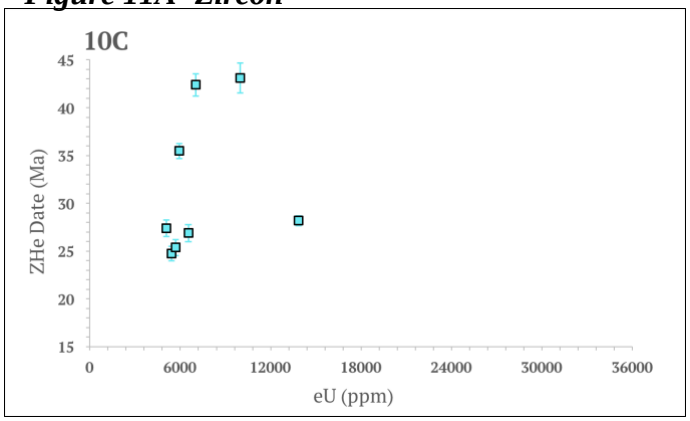

Figure 11B- Zircon

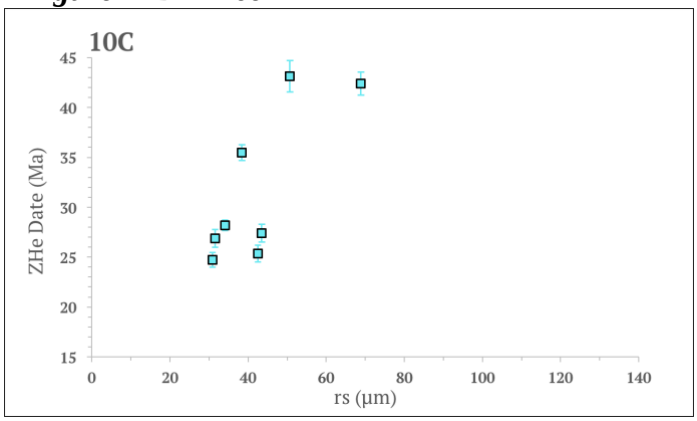

Figure 12A- Apatite

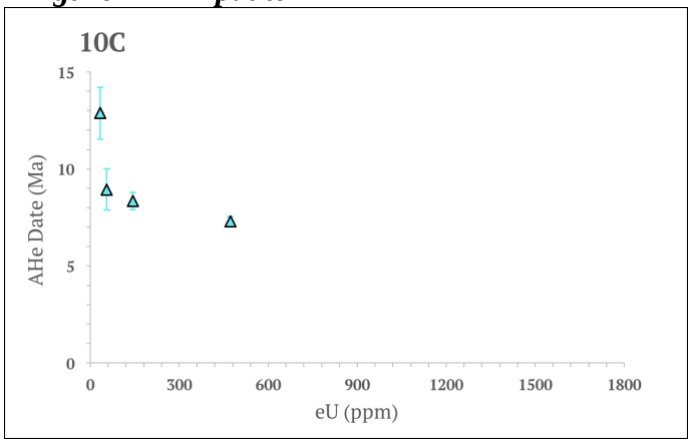

Figure 12B- Apatite

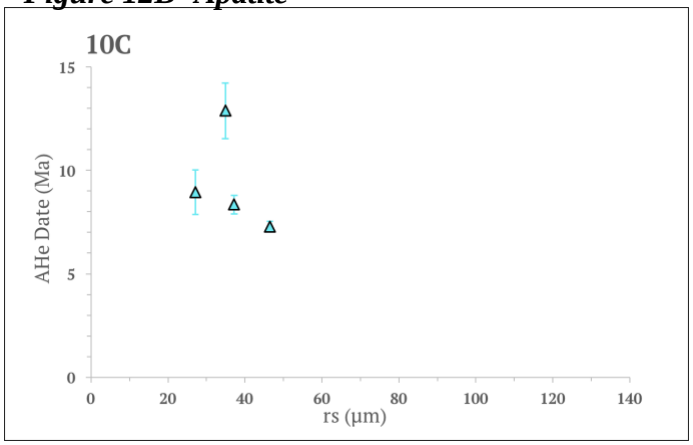

Figure 13A

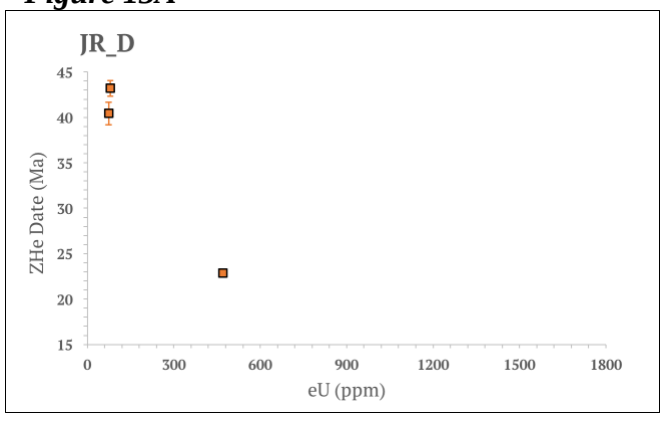

Figure 13B

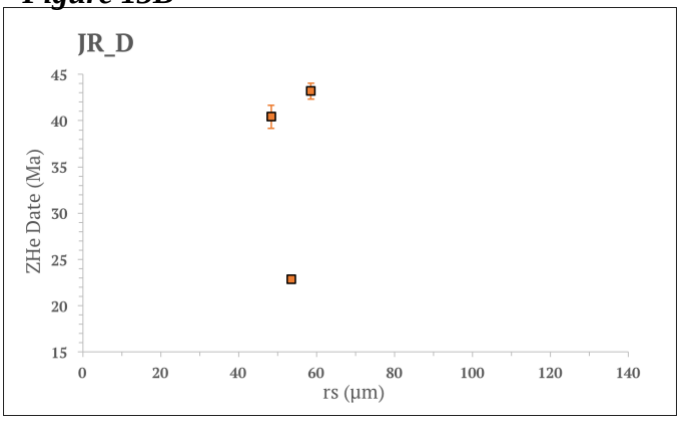

DISCUSSION

There are three key factors that largely influence age date variations in a zircon sample: accumulated radiation damage (eU), grain size, and U-Th zonation. When all zircons in a sample have experienced the same integrated thermal history, eU can be used as a proxy for accumulated radiation damage (e.g. Flowers et al., 2009; Guenthner et al., 2013). Interpreting date-eU correlations in each sample was essential in better understanding the exhumation path of this complex.

He diffusivity in zircon abruptly increases once it reaches a specific threshold of radiation damage of about 2 X 10^{18} α/g (Guenthner et al., 2013). Rapid He diffusion is achieved through interconnected damage-zones when zircons sustain long-term radiation damage accumulation either at temperatures low enough to prevent annealing or at surface temperatures that cause resetting and significant He loss (Guenthner, 2013). These scenarios result in negative date-eU correlations, which RGD17-35, JR_K, and JR_J exhibit. RGD17-35 has exceptionally high eU concentrations and displays a similar pattern.

The flat date-eU correlations in JR_S and RGD17-31 are inidicative of two separate rapid cooling events: one at ~20 Ma recorded in RGD17-31 and the other at ~40 Ma recorded in JR_S. Our oldest cooling dates are consistent with $^{40}Ar/^{39}Ar$ ages that range from 39.0 to 42.6 Ma from 12 different locations including the northern Pequop Mountains, the northern/southern East Humboldt Range, and the Wood Hills (Thorman and Snee, 1995), as well as $^{40}Ar/^{39}Ar$ and ZHe dates from the Southern East Humboldt Range (e.g. McGrew et al., 2019 and Metcalf et al., 2019). Futhermore, our ~20 Ma dates are consistent with zircon fission track ages from the Harrison Pass pluton in the Ruby Mountains (Reese, 1986), as well as $^{40}Ar/^{39}Ar$, ZHe, and AHe data from the Ruby Mountains and East Humboldt Range (e.g. McGrew et al., 2019 and Metcalf

et al., 2019).

My apatite dates range from 8 to 13 Ma and are consistent with AHe ages obtained in the southern Ruby Mountains interpreted by Colgan et al. (2010) to record rapid unroofing accommodated by a west dipping detachment fault that bounds the west side of the Ruby Mountains and East Humboldt Ranges.

I performed thermal history modeling of representative zircon and apatite data from sample 10C (Figure 14) to test my data within geologic constraints defined by other studies. I also attempted to modeled JR_J and RGD17-31; however, HeFTy could not fit the negative date-eU patterns in the ZHe data at the same time, and the outputs were therefore unreliable. The model had a difficult time fitting time-temperature paths that could produce the amount of accumulated radiation damage needed to create a negative date-eU correlation within the prescribed geologic constraints for sample JR_J. Recent work suggests that radiation damage in zircon may require higher temperatures to anneal than are included in the Guenthner model (Ginster et al., 2019), which may be the cause of this discrepancy. Similarly, we modeled sample 10C using only one group of ZHe data (low eU) (Figure 14). 10C yielded a modeled ZHe age of 26.1 Ma with a ZHe alpha accumulation of 9.979 x 10_{17} α/g. This alpha dose correlates to a closure temperature of ~180°C based on Guenthner et al. (2013) and implies that these zircons passed through a closure temperature of ~180°C at ~26.1 Ma. 10C yielded a AHe date of 10.1 Ma combined with an apatite closure temperature range of ~60 to 70°C implies that this apatite system passed through its closure temperature at ~10 Ma. A model using both low and high eU ZHe and AHe data (Figure 15) produced similar results to our initial model and suggests that exhumation and extension was going on by at least 40 Ma.

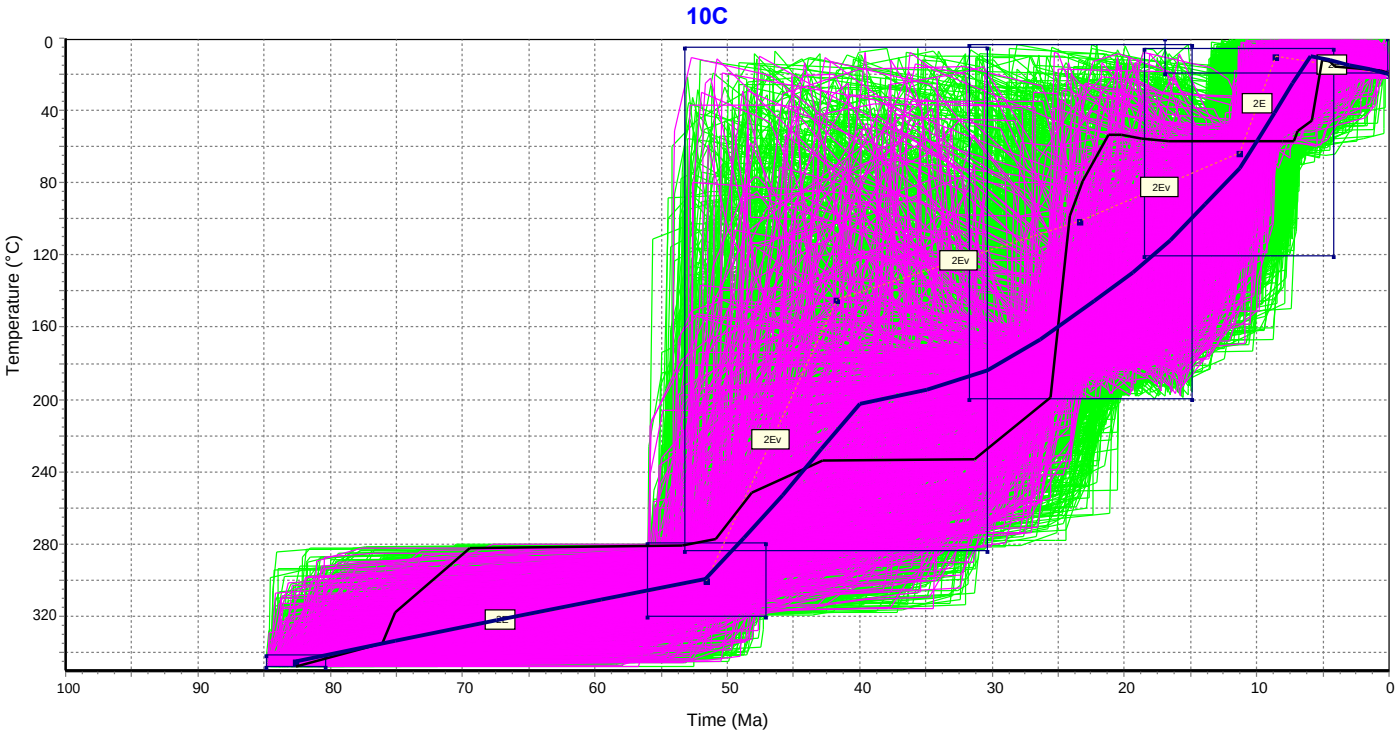

Figure 14. *Thermal history model for 10C with low eU zircon and apatite data. Green lines depict "acceptable fit" time-temperature paths and purple lines represent "good fit" time-temperature paths.*

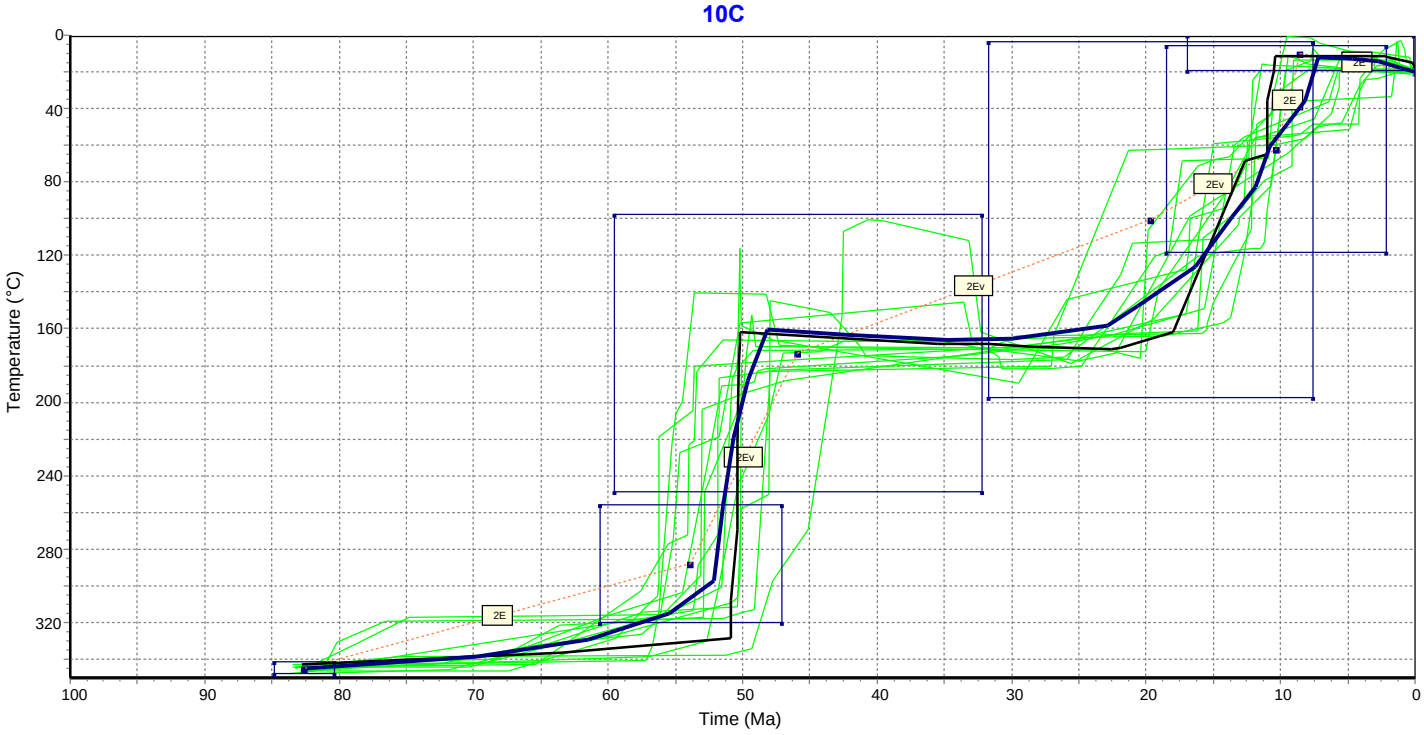

Figure 15. *Thermal history model for 10C using low and high eU zircon and apatite data. Only green lines of "acceptable fit" were generated.*

Taken together, these new data and models suggest that the Wood Hills experienced a multistep exhumational and cooling history that tends to young from southeast to northwest. Obtaining more apatites in the future will help to better constrain the thermal history of this complex through ~60-70°C. Additionally, acquiring more zircons for samples like JR_D and JR_K that lack zircon dates will also provide a more comprehensive exhumational history. With recent work investigating whether accumulated radiation damage in zircon requires higher temperatures to anneal than expected, thermal modeling software like HeFTy will become better equipped to fit more complex time-temperature paths with high eU like those seen in our data.

Table 1. Zircon (U-Th)/He Results

Sample Name	L1 (um)	W1 (um)	L2 (um)	W2 (um)	Rs (um)	4He (nmol/g)	U (ppm)	Th (ppm)	Sm (ppm)	eU (ppm)	Raw Date (Ma)	Ft	Corr. Date (Ma)	Analytic Unc. (Ma) 2σ
RGD17-31_z01	127.8	49.5	127.7	75.2	34.88	1.447	31.63	7.95	70.70	33.5	7.88	0.606	12.88	1.34
RGD17-31_z02	145.1	88.4	143.3	96.4	48.76	23.585	235.21	109.99	0.68	261.1	16.73	0.768	24.28	0.65
RGD17-31_z03	148.8	103.5	156.8	69.3	47.79	30.018	256.48	169.15	0.74	296.2	18.76	0.764	27.29	4.02
RGD17-31_z04	329.2	126.6	331.3	127.0	79.72	150.687	1447.47	20.77	0.19	1452.4	19.23	0.857	22.42	0.60
RGD17-31_z05	192.5	81.5	194.0	71.5	47.55	24.779	310.91	26.95	1.64	317.2	14.48	0.765	18.91	0.86
RGD17-31_z06	297.9	125.8	297.5	134.3	79.65	181.904	1740.96	36.50	1.36	1749.5	19.27	0.858	22.46	0.71
RGD17-31_z07	277.5	108.8	275.3	106.8	67.54	117.300	1191.39	35.27	1.95	1199.7	18.13	0.832	21.76	0.76
RGD17-31_z08	454.0	236.9	476.1	204.8	132.2	137.606	1346.14	22.48	0.72	1351.4	18.88	0.913	20.67	0.96
RGD17-31_z09	200.3	189.6	109.9	166.7	84.48	6.771	42.90	94.30	19.40	65.1	19.18	0.853	22.47	2.97
RGD17-32_z01	476.6	124.1	458.4	163.0	92.38	109.316	1126.19	243.60	1.43	1183.4	17.12	0.875	19.55	0.47
RGD17-32_z02	176.9	156.7	162.2	165.5	81.84	54.819	469.15	166.82	0.69	508.4	19.97	0.855	23.35	0.93
RGD17-32_z03	148.8	102.3	159.6	93.9	55.06	79.731	636.70	166.55	1.12	675.8	21.85	0.786	27.78	0.77
RGD17-35_z01	270.5	144.5	269.9	143.8	82.56	3068.151	23505.3	1159.1	5.55	23778	23.91	0.862	34.46	0.51
RGD17-35_z02	177.1	78.0	166.9	85.4	49.06	3805.397	34743.0	1658.8	10.88	35133	20.08	0.774	28.94	1.18
RGD17-35_z03	203.3	120.5	205.1	165.0	74.95	1239.624	6375.55	481.89	2.25	6488.8	35.36	0.849	41.61	1.15
RGD17-35_z04	185.5	83.5	183.4	77.3	49.24	1337.831	14827.9	747.60	3.28	15004	16.53	0.775	21.32	0.45
JR_D_z01	166.3	99.6	165.0	94.8	53.56	45.975	461.55	39.23	7.02	470.8	18.0	0.791	22.88	0.34
JR_D_z02	143.1	99.6	135.5	75.5	48.36	12.134	61.41	52.14	2.70	73.7	30.45	0.752	40.43	1.25
JR_D_z03	171.3	114.7	166.6	112.9	58.58	15.011	70.23	40.55	0.00	79.8	34.80	0.805	43.21	0.86
JR_J_z01	301.6	107.8	307.3	101.8	67.29	15.561	71.46	33.10	0.55	79.2	36.31	0.829	43.76	0.61
JR_J_z02	270.3	94.5	272.6	94.4	60.58	26.555	183.36	44.39	1.23	193.8	25.37	0.813	31.21	0.43
JR_J_z03	254.9	90.0	257.7	96.3	59.17	11.462	65.13	39.25	0.00	74.4	28.52	0.806	35.36	0.53
JR_J_z04	174.6	163.5	169.5	164.1	83.22	49.071	289.86	344.24	2.60	370.8	24.47	0.854	28.65	0.97
JR_J_z05	140.4	95.2	136.9	102.8	49.10	66.945	708.55	41.88	0.64	718.4	17.28	0.773	22.32	0.49
JR_K_z01	239.0	146.4	236.7	147.4	79.12	28.799	167.07	53.77	0.00	179.7	29.66	0.855	34.68	0.49
JR_K_z02	160.0	107.2	158.3	103.9	54.78	10.101	59.67	26.71	0.00	65.9	28.35	0.793	35.73	0.80
JR_K_z03	163.3	125.2	176.7	121.5	60.63	34.034	232.31	21.61	0.00	237.4	26.55	0.814	32.59	0.45
JK_O_z01	204.6	148.3	203.1	137.2	78.59	14.015	95.56	49.90	1.04	107.3	24.18	0.848	28.49	0.40
JR_O_z02	245.5	118.3	247.7	117.2	69.36	13.332	95.86	48.50	0.00	107.3	23.01	0.828	27.76	0.46
JR_O_z03	186.6	101.3	187.3	101.0	58.54	18.162	143.78	113.69	2.58	170.5	19.72	0.795	24.79	0.33
JR_O_z04	142.4	73.3	127.1	68.0	41.42	23.366	174.93	96.83	0.56	197.7	21.88	0.731	29.88	1.12
JR_O_z05	116.4	79.6	123.6	78.9	44.24	14.381	131.79	98.84	1.30	155.0	17.17	0.730	23.49	0.82
JR_O_z06	133.3	68.1	131.0	64.7	38.82	69.111	643.43	114.88	1.71	670.4	19.10	0.700	27.27	0.67
JR_O_z07	154.3	93.7	154.6	84.0	50.73	23.701	190.22	130.97	2.21	221.0	19.85	0.765	25.94	0.97
JR_S_z01	187.4	141.1	186.5	141.3	76.48	8.734	42.87	19.07	0.00	47.3	34.12	0.844	40.38	0.79
JR_S_z02	176.4	149.1	168.6	153.1	78.71	17.554	76.71	76.37	5.04	94.7	34.26	0.846	40.46	0.54
JR_S_z03	175.6	133.1	165.8	139.6	72.81	15.192	83.08	33.68	4.48	91.0	30.88	0.837	36.87	0.60
JR_S_z04	157.7	140.7	157.4	145.6	73.75	15.568	85.73	30.20	0.00	92.8	31.04	0.830	36.96	0.56
JR_S_z05	147.9	122.6	148.3	117.8	63.93	70.392	340.38	235.67	4.20	395.8	32.89	0.813	40.43	1.23
JR_S_z06	111.4	88.8	115.9	89.0	47.75	27.873	155.11	117.42	0.61	182.7	28.22	0.750	37.59	2.44
JR_S_z07	103.2	107.3	117.2	82.9	48.99	45.396	238.00	157.67	0.76	275.1	30.53	0.757	40.30	0.82
10C_z01	188.2	55.1	191.6	39.2	30.88	470.696	5405.11	93.24	1.05	5427.0	16.08	0.650	24.73	0.74
10C_z02	204.9	65.9	206.7	47.7	34.08	1393.694	13778.2	302.92	3.92	13849	18.65	0.661	28.18	0.51
10C_z03	157.8	49.7	155.7	47.1	31.53	626.728	6513.35	112.11	6.26	6539.7	17.77	0.660	26.88	0.90
10C_z04	239.7	65.0	240.6	62.0	42.50	577.400	5672.87	105.58	1.68	5697.9	18.79	0.740	25.37	0.84
10C_z05	207.2	65.6	205.6	51.9	38.39	812.385	5882.56	237.99	3.65	5938.5	25.34	0.713	35.48	0.78
10C_z06	298.6	60.1	272.8	67.7	43.48	558.750	5051.45	74.61	0.96	5069.0	20.43	0.745	27.39	0.88
10C_z07	346.7	123.3	346.0	92.5	68.89	1346.785	6952.30	318.00	2.67	7027.0	35.47	0.836	42.40	1.15
10C_z08	205.3	79.3	215.9	81.9	50.72	1817.746	9822.98	677.95	4.22	9982.3	33.71	0.781	43.12	1.56

Table 2. Apatite (U-Th)/He Results

Sample Name	L1 (um)	W1 (um)	L2 (um)	W2 (um)	Rs (um)	4He (nmol/g)	U (ppm)	Th (ppm)	Sm (ppm)	eU (ppm)	Raw Date (Ma)	Ft	Corrected Date (Ma)	Analytic Unc.. (Ma) 2σ
10C_a01	127.8	49.5	127.7	75.2	34.88	1.447	31.63	7.95	70.70	33.5	7.88	0.606	12.88	1.34
10C_a02	145.7	62.0	147.4	68.3	37.19	4.102	141.75	7.96	60.13	143.6	5.38	0.631	8.35	0.44
10C_a03	103.4	80.6	104.9	98.7	46.49	12.972	469.29	10.46	61.52	471.7	5.10	0.699	7.29	0.25
10C_a04	77.4	49.7	77.8	55.7	27.12	1.397	54.74	3.51	36.91	55.6	4.64	0.517	8.94	1.07

WORKS CITED

1. Camilleri, P., 2010, Geologic Map of the Wood Hills, Elko County, Nevada: Nevada Bureau of Mines and Geology, Map 172, 1:48,000, with companion text, 16 p.
2. Camilleri, P.A., and Chamberlain, K.R., 1997, Mesozoic tectonics and metamorphism in the Pequop Mountains and Wood Hills region, northeast Nevada: Implications for the architecture and evolution of the Sevier orogen (vol 109, pg 74, 1997): Geological Society of America Bulletin, v. 109, no. 4, p. 504.
3. Colgan, J.P., Howard, K.A., Fleck, R.J., and Wooden, J.L., 2010, Rapid middle Miocene extension and unroofing of the southern Ruby Mountains, Nevada: Tectonics, v. 29, no. 6, p. TC6022.
4. Farley, K.A., 2000, Helium diffusion from apatite: General behavior as illustrated by Durango fluorapatite: Journal of Geophysical Research-Solid Earth, v. 105, p. 2903–2914.
5. Farley, K.A., Wolf, R., and Silver, L., 1996, The effects of long alpha-stopping distances on (U-Th)/He ages: Geochmica et Cosmochimica Acta, v. 60, p. 4223–4229.
6. Flowers, R.M., Ketcham, R.A., Shuster, D.L., and Farley, K.A., 2009, Apatite (U–Th)/He thermochronometry using a radiation damage accumulation and annealing model: Geochmica et Cosmochimica Acta, v. 73, p. 2347–2365, doi: 10.1016/j.gca.2009.01.015.
7. Ginster, U., Reiners, P.W., Nasdala, L., N, C.C., 2019. Annealing kinetics of radiationdamage in zircon. Geochem. Cosmochim. Acta 249, 225–246
8. Guenthner, W.R., Reiners, P.W., Ketcham, R.A., Nasdala, L., and Giester, G., 2013, Helium diffusion in natural zircon: Radiation damage, anisotropy, and the interpretation of zircon (U-Th)/He thermochronology: American Journal of Science, v. 313, p. 145–198, doi: 10.2475/03.2013.01.
9. Hendriks, B.W.H. “Analytical Methods/Fission Track Analysis”. *Encyclopedia of Geology,* 2005.
10. Hiess, J., Condon, D.J., Mclean, N., and Noble, S.R., 2012, U-238/U-235 Systematics in Terrestrial Uranium-Bearing Minerals: Science, v. 335, p. 1610–1614, doi: 10.1126/science.1215507.

11. Holland, H. D., 1954, Radiation damage and its use in age determination, in Faul, H., editor, Nuclear Geology: New York, Wiley, p. 175–179.
12. Hurley, P. M., 1954, The helium age method and the distribution and migration of helium in rocks, in Faul, H., editor, Nuclear Geology: New York, Wiley, p. 301–329.
13. Ketcham, R. A., Gautheron, C., & Tassan-Got, L. (2011). Accounting for long alpha-particle stopping distances in (U-Th-Sm)/He geochronology: Refinement of the baseline case. *Geochmica Et Cosmochimica Acta*, *75*(24), 7779–7791. http://doi.org/10.1016/j.gca.2011.10.011
14. Lund Snee, J.E., Miller, E.L., Grove, M., Hourigan, J.K., and Konstantinou, A., 2016, Cenozoic paleogeographic evolution of the Elko Basin and surrounding region, northeast Nevada: Geosphere, v. 12, p. 464–500, doi: 10.1130/GES01198.S1.
15. McGrew, A. J., M. T. Peters, and J. E. Wright (2000), Thermobarometric constraints on the tectonother- mal evolution of the East Humboldt Range meta- morphic core complex, Nevada, Geol. Soc. Am. Bull.,
16. McGrew, A.J., Snoke, A.W., 2015, Geologic map of the Welcome quadrangle and an adjacent part of the Wells quadrangle, Elko County, Nevada: Nevada Bureau of Mines and Geology Map 184, scale 1:24,000, 40 p.
17. Metcalf, J.R., Flowers, R. M., 2019 "(U-Th)/He chronometer, in press, Encyclopedia of Geology, Elsevier Press.
18. Nasdala, L., Reiners, P. W., Garver, J. I., Kennedy, A. K., Stern, R. A., Balan, E., and Wirth, R., 2004a, Incomplete retention of radiation damage in zircon from Sri Lanka: American Mineralogist, v. 89, p. 219–231.
19. Reese, N. M. (1986), Cenozoic tectonic history of the Ruby Mountains and adjacent areas, Northeastern Nevada: Constraints from radiometric dating and seismic profiles, M.S. thesis, 87 pp., Southern Methodist Univ., Dallas, Tex.
20. Reiners, P.W., and Farley, K.A., 1999, Helium diffusion and (U-Th)/He thermochronometry of titanite: Geochmica et Cosmochimica Acta, v. 63, p. 3845–3859.
21. Satarugsa, P., and Johnson, R.A., 2000, Cenozoic tectonic evolution of the Ruby Mountains metamorphic core complex and adjacent valleys, northeastern Nevada: Rocky Mountain Geology, v. 35, p. 205–230.

22. Thorman, C.H., 1970, Metamorphosed and nonmetamorphosed Paleozoic rocks in the Wood Hills and Pequop Mountains, northeast Nevada: Geological Society of America Bulletin, v. 81, p. 2417–2448.
23. Thorman, C. H., and Snee, L. W., 1988, Thermochronology of metamor- phic rocks in the Wood Hills and Pequop Mountains, northeastern Nevada: Geological Society of America Abstracts with Programs, v. 20, no. 7, p. A18.
24. Wolf, R., Farley, K.A., and Kass, D., 1998, Modeling of the temperature sensitivity of the apatite (U-Th)/He thermochronometer: Chemical Geology, v. 148, p. 105–114.
25. Wolfe, Franklin, 2016, New Constraints on the Timing, Rate, and Style of Exhumation of the Wood Hills and Pequop Mountains, Elko County, Nevada, Honors Thesis, Washington and Lee University, 71 pp.